Eur. Phys. J. B **25**, 519–529 (2002)
DOI: 10.1140/epjb/e20020057

THE EUROPEAN PHYSICAL JOURNAL B
EDP Sciences

Coarsening process in one-dimensional surface growth models

Alessandro Torcini[1,2,a] and Paolo Politi[2,b]

[1] Dipartimento di Energetica "S. Stecco", Università di Firenze, Via S. Marta 3, 50139 Firenze, Italy
[2] Istituto Nazionale per la Fisica della Materia, UdR Firenze, Via G. Sansone 1, 50019 Sesto Fiorentino, Italy

Received 28 September 2001 and Received in final form 21 November 2001

Abstract. Surface growth models may give rise to instabilities with mound formation whose typical linear size L increases with time (coarsening process). In one dimensional systems coarsening is generally driven by an attractive interaction between domain walls or kinks. This picture applies to growth models for which the largest surface slope remains constant in time (corresponding to model B of dynamics): coarsening is known to be logarithmic in the absence of noise ($L(t) \sim \ln t$) and to follow a power law ($L(t) \sim t^{1/3}$) when noise is present. If the surface slope increases indefinitely, the deterministic equation looks like a modified Cahn-Hilliard equation: here we study the late stages of coarsening through a linear stability analysis of the stationary periodic configurations and through a direct numerical integration. Analytical and numerical results agree with regard to the conclusion that steepening of mounds makes deterministic coarsening *faster*: if α is the exponent describing the steepening of the maximal slope M of mounds ($M^\alpha \sim L$) we find that $L(t) \sim t^n$: n is equal to $\frac{1}{4}$ for $1 \leq \alpha \leq 2$ and it decreases from $\frac{1}{4}$ to $\frac{1}{5}$ for $\alpha \geq 2$, according to $n = \alpha/(5\alpha - 2)$. On the other side, the numerical solution of the corresponding stochastic equation clearly shows that in the presence of shot noise steepening of mounds makes coarsening *slower* than in model B: $L(t) \sim t^{1/4}$, irrespectively of α. Finally, the presence of a symmetry breaking term is shown not to modify the coarsening law of model $\alpha = 1$, both in the absence and in the presence of noise.

PACS. 68. Surfaces and interfaces – 81.10.Aa Theory and models of film growth – 02.30.Jr Partial differential equations

1 Introduction

In real systems, surface growth occurs on two-dimensional (2d) substrates and therefore its modelization in one dimension (1d) is in general an oversimplification, mainly justified by the possibility of obtaining a deeper understanding of the dynamical evolution of the system. In some cases the surface indeed maintains a 1d profile, for example when the relaxation of a grooved surface is studied [1]. This is not true when the surface undergoes kinetic roughening or a growth instability followed by a phase separation: in both cases, noise makes the resulting morphology 2d even if the initial one is 1d. The dynamic evolution of a vicinal surface is another possible application of 1d models. In fact, if atomic steps move in phase [2], step motion is described by a one-dimensional growth equation.

In this paper we are interested in a growing surface that undergoes a kinetic instability. The origin of such an instability is related to an additional barrier that diffusing adatoms must overcome to descend step edges (the so-called Ehrlich-Schwoebel (ES) barrier [3,4]). Even in the presence of stabilizing mechanisms, at sufficiently large scales the ES effect can be the dominant one and the flat surface becomes unstable against small deformations. In a first linear regime, a structure with a well-defined wavelength emerges and its amplitude increases in time. At a later stage, nonlinearities come into play and the mound structure typically – but not unavoidably [2] – coarsens.

This simplified picture resembles spinodal decomposition and coarsening that take place during phase separation. Surface growth instability and phase separation do have strong similarities and they can indeed be equivalent in 1d [5]. However, they are definitely different in two dimensions [6].

Generally speaking, phase separation has different properties in one and two dimensions. We mention here two of them [7]: (i) In 2d, coarsening is driven by the tension of domain walls while in 1d it is due to interaction between the walls. (ii) Noise is generally irrelevant in 2d, while it modifies the coarsening law in 1d (except in the presence of long-range interactions).

The class of models that we study in one dimension is of interest in two respects. First, since the slope is assumed to increase indefinitely, it is not possible to speak of domain walls between different phases. Second, being that the interaction is long ranged, noise may happen to be irrelevant for the coarsening law in 1d: this occurs for some of the models studied here.

[a] e-mail: torcini@ino.it
[b] *Corresponding author:* politi@fi.infn.it

In the next section we give a short introduction to the continuum equations that are encountered in one-dimensional models of conserved surface growth. A more detailed analysis can be found in recent review papers [5,8]. In Section 3 we recall a few theoretical approaches to one-dimensional coarsening and in Section 4 we apply the linear stability analysis to our class of deterministic α-models. Its results are confirmed by numerics. The problem of coarsening in the presence of noise is addressed directly *via* stochastic numerical integration in Section 5. In Section 6 we examine the effect of a symmetry breaking term, while the discussion of the results and our conclusions are presented in the final section.

2 Models for unstable surface growth

In the Introduction we have already mentioned the ES barriers as a source of the kinetic instability. In fact, it is well-known [9] that an asymmetry in the sticking coefficients of an adatom to a step produces a slope-dependent current $j_{\rm ES}(m)$; $h(x,t)$ and $m=\partial_x h$ are the local height and slope of the surface. It is more convenient to use the variable $z(x,t)=h(x,t)-\bar{h}$, where $\bar{h}=F_0 t$ is the average height, instead of $h(x,t)$ (F_0 being the intensity of the flux). In this way the evolution equation $\partial_t h = F_0 - \partial_x j$ simply writes as $\partial_t z = -\partial_x j$ while the definition of the slope $m=\partial_x h = \partial_x z$ is unaffected.

For symmetry reasons, $j_{\rm ES}$ is an odd function of m. Therefore we expect that $j_{\rm ES} \simeq \nu m$ at small slopes, as confirmed by a more rigorous analysis [5]. The asymmetry in the sticking coefficients is generally due to the additional energy barrier hindering the adatom from descending a step. This gives rise to an up-hill current $j_{\rm ES} \simeq \nu m$ with a positive coefficient ν. This implies that $j_{\rm ES}$ has a destabilizing character, as easily revealed by the solution of the linear differential equation $\partial_t z = -\partial_x j_{\rm ES} = -\nu \partial_x^2 z(x,t)$: $z(x,t) = z_0 \cos(qx) \mathrm{e}^{\omega_q t}$, with $\omega_q = \nu q^2$.

In a continuum model, where the lattice constant a goes to zero, the following expression for $j_{\rm ES}$ can be used:

$$j_{\rm ES} = \frac{\nu m}{1+\ell_{\rm D}^2 m^2} \qquad \text{model 1.} \tag{1}$$

If a discrete model with square symmetry is used, we expect $j_{\rm ES}$ to vanish for $m=m_0=1/a$. We can therefore define the model:

$$j_{\rm ES} = \nu m (1-m^2/m_0^2) \quad \text{model 0.} \tag{2}$$

However, other mechanisms can produce a slope-dependent current: short-range step-adatom interaction [3,10], post-deposition transient mobility and downward funneling [11]. The first mechanism may be either stabilizing or not, depending on the sign of the step-adatom interaction while the other (non-thermal) mechanisms are typically stabilizing, *i.e.* they contribute with a negative term $-\nu' m$ to $j_{\rm ES}$. Because of that, either the ES current acquires a zero at finite slope (from model 1 we pass to model 0) or there is a change in the value m_0 at which $j_{\rm ES}$ vanishes.

Finally, in a previous paper [12] we have generalized equation (1) to a class of models (α-models) characterized by different asymptotic behaviors for $m \to \infty$:

$$j_{\rm ES} = \frac{\nu m}{(1+\ell_{\rm D}^2 m^2)^\alpha} \qquad \text{model } \alpha \ (\geq 1) \ . \tag{3}$$

In the Introduction we also mentioned possible stabilizing mechanisms. The simplest expression for a stabilizing current is the so-called Mullins term that in its linearized form reads $j_{\rm M} = K\partial_x^2 m$. Its origin may be either thermodynamic (relaxation through surface diffusion [13]) or kinetic (fluctuations in the nucleation process of new islands [14,15]). A stabilizing current gives a negative contribution to ω_q. Starting from the equation $\partial_t z = -\partial_x (j_{\rm ES} + j_{\rm M})$ it is easily found that $\omega_q = \nu q^2 - K q^4$. A flat surface is thereby linearly unstable against fluctuations of wavelength larger than $\lambda_c = 2\pi\sqrt{K/\nu}$.

Both currents $j_{\rm ES}$ and $j_{\rm M}$ change sign if $x \to -x$ or $z \to -z$: the growth process cannot break the former symmetry but it does break the latter. It has been shown [9,14] that such symmetry breaking term (intrinsically nonlinear) has the form $j_{\rm SB} = \partial_x A(m^2)$, where $A \sim m^2$ at small slopes and $A \sim -1/m^2$ at large ones. Its presence is strictly related to the breaking of the detailed balance principle [16] and therefore to the non-equilibrium character of the growth process.

It has been proven [17] that $j_{\rm SB}$ does not modify the coarsening law of model 0: the effects of $j_{\rm SB}$ on model 1 will be considered in Section 6.

We conclude this section by writing down explicitly the class of growth equations that are analyzed in the paper:

$$\partial_t z(x,t) = -\partial_x j(x,t) + \eta(x,t) \tag{4}$$

$$j(x,t) = \begin{cases} \partial_x^2 m + \frac{m}{(1+m^2)^\alpha} & \text{model } \alpha \\ \partial_x^2 m + m(1-m^2) & \text{model 0} \end{cases} \tag{5}$$

$$\langle \eta(x,t) \rangle = 0 \quad \langle \eta(x,t)\eta(x',t') \rangle = \tilde{F}_0 \delta(x-x')\delta(t-t'). \tag{6}$$

Equation (4) is the evolution equation of the local height $z(x,t)$ for a conserved growth process in the presence of the shot noise $\eta(x,t)$; equations (5) give the currents for the α-models and model 0, once that x,t,z have been rescaled in order to get an adimensional equation. Equation (6) gives the spectral properties of the noise, whose strength $\tilde{F}_0 = F_0 a \ell^2/\sqrt{\nu K}$ is the only parameter appearing in the problem: F_0 is the intensity of the flux, a is the lattice constant, ℓ is the diffusion length $\ell_{\rm D}$ for α-models (Eqs. (1, 3)) or the inverse of the constant slope m_0 for model 0 (Eq. (2)), ν and K are the prefactors of $j_{\rm ES}$ and $j_{\rm M}$, respectively.

3 Theoretical approaches to coarsening

In this section we review two theoretical methods that have been used to study the coarsening process in model 0.

The first method uses the property that the current $j_{\rm ES}$ vanishes at a finite slope m_0. Although it can not be used for α-models, for completeness and clarity we discuss it in Section 3.1. The second method consists in a linear stability analysis of the stationary configurations. It is a very general method and it is discussed in Section 3.2. In the context of phase separation processes it was introduced by Langer [20] to study model 0 and its solution is proposed in Section 4.1. Its application to α-models is carried out in Section 4.2.

3.1 Kink dynamics

Model 0 and α-models have the same linear behaviour, but they strongly differ in the nonlinear regime: in model 0 the slope increases up to the maximal value $m_0 = \pm 1$ while in α-models it grows indefinitely.

For model 0, the surface profile corresponding to a constant value $m_0 = 1$ (*i.e.* a vicinal surface with unitary slope) is stable [18], but it can not be attained starting from a flat surface because the average slope must remain constant. Still, we can consider the stationary configuration $m_+(x)$ ($j(m_+(x)) \equiv 0$) corresponding to a limiting slope $\pm m_0$ for $x \to \mp\infty$. That profile is called 'mound' in the z-space and 'kink' or 'domain wall' in the space of the order parameter m, where it has the form $m_+(x) = \tanh(x/\sqrt{2})$.

During the coarsening process of model 0 a typical surface profile is just an alternating sequence of kinks ($m = m_+(x)$) and antikinks ($m = m_-(x) = -m_+(x)$), whose average distance $L(t)$ increases with time because of the annihilation process between pairs of neighbouring kink-antikink. In the absence of noise the dynamics of kinks is governed by their attractive interaction that decays exponentially with the distance, since $|m_\pm(x)| \simeq 1 - 2\exp(-\sqrt{2}|x|)$ for $|x| \gg 1$. Such a weak interaction determines a very slow coarsening: $L(t) \sim \ln t$ [19,20].

In the presence of noise the picture is different because of the induced fluctuations on the kink positions. If there were no constraint induced by the conservation of the order parameter, kinks would simply perform a random walk and therefore would travel a distance L in a typical time L^2, giving a coarsening exponent $n = 1/2$ ($L(t) \sim \sqrt{t}$). In a growth process, where a conservation law does exist, kink trajectories are not independent and the coarsening slows down: $n = 1/3$. This exponent is more easily understood in a spin picture [21], where the conservation of the order parameter (the magnetization) implies that the system evolves through spin-exchange processes (Kawasaki dynamics).

If we now turn to α-models, we recognize that the kink picture is not applicable because the unstable current $j_{\rm ES}$ vanishes for infinite slope only.

3.2 Linear stability analysis of stationary configurations

We now discuss the linear stability analysis of the stationary configurations. They are determined by the condition

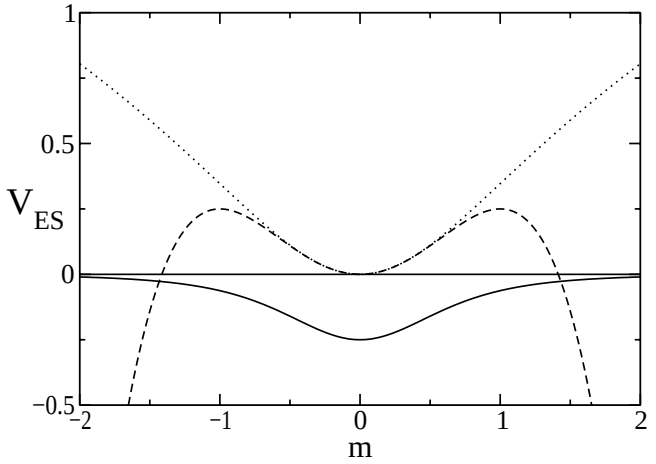

Fig. 1. Profiles of the different potentials $V_{\rm ES}$. From top to bottom: Model 1 (dotted line), equation (9); Model 0 (dashed line), equation (8); Model $\alpha = 3$ (full line), equation (10).

$\partial_t z(x,t) \equiv 0$, *i.e.* the current must be a constant: $j \equiv c$. The net current c is related to the average slope of the surface: we are interested in a high symmetry surface and therefore we set $c = 0$.

The equation $j = 0$ is formally equal to the Newton's equation for a particle of unitary mass, where the slope m plays the role of the particle position and x the role of time:

$$\partial_x^2 m(x) + j_{\rm ES}(m) = 0 \ . \tag{7}$$

The fictitious particle feels the force $-j_{\rm ES}(m)$, *i.e.* it moves in the potential $V_{\rm ES}(m) = \int^m {\rm d}s j_{\rm ES}(s)$. Different models give qualitatively different potentials (see Fig. 1):

$$V_{\rm ES}(m) = \quad m^2/2 - m^4/4 \qquad \text{model 0} \tag{8}$$

$$V_{\rm ES}(m) = \quad (1/2)\ln(1+m^2) \qquad \text{model 1} \tag{9}$$

$$V_{\rm ES}(m) = -(1+m^2)^{1-\alpha}/[2(\alpha-1)] \quad \text{model } \alpha > 1. \tag{10}$$

Stationary configurations therefore correspond to the periodic oscillations of the particle around the minimum of $V_{\rm ES}$ in $m = 0$. We label the stationary configurations $m_{\rm 2L}(x)$ through their period $2L$. What about the limit $L \to \infty$? For model 0 it corresponds to the kink-solution: $m_\infty(x) = m_+(x) \to \pm 1$ when $x \to \pm\infty$. For model 1, the energy of the particle diverges when the period L increases and the limiting configuration $m_\infty(x)$ does *not* exist. It does exist for $\alpha > 1$ and it corresponds to the well defined problem of a particle of zero energy moving in the potential (10): it starts at $m = -\infty$ and arrives at $m = +\infty$ after an infinite time.

We start by considering small deviations ψ from the periodic profile: $m(x,t) = m_{\rm 2L}(x) + \psi(x,t)$. Since $j_{\rm ES}(m_{\rm 2L} + \psi) = j_{\rm ES}(m_{\rm 2L}) + j'_{\rm ES}(m_{\rm 2L})\psi + \mathcal{O}(\psi^2)$, we obtain that the linearized evolution equation for $\psi(x,t)$ is

$$\partial_t \psi = \partial_x^2 \left[-\psi''(x,t) - j'_{\rm ES}(m_{\rm 2L}(x))\psi\right] \tag{11}$$

and therefore the time dependence of ψ is: $\psi(x,t) = \phi(x) \cdot \exp(-\epsilon t)$. Replacing the expression of ψ in terms of ϕ into

equation (11), we find that the stability is determined by the spectrum of the following operator:

$$(-\partial_x^2)\left[-\phi''(x) + U_{\rm L}(x)\phi\right] \equiv D_x\hat{H}\phi(x) = \epsilon\phi \ , \qquad (12)$$

where $D_x \equiv -\partial_x^2$ and $\hat{H} \equiv -\partial_x^2 + U_{\rm L}(x)$ is a single-particle Schrödinger operator corresponding to the periodic potential $U_{\rm L}(x) \equiv -j'_{\rm ES}(m_{\rm 2L}(x))$, *of period* L:

$$\begin{aligned} U_{\rm L}(x+L) &= -j'_{\rm ES}(m_{\rm 2L}(x+L)) \\ &= -j'_{\rm ES}(-m_{\rm 2L}(x)) = U_{\rm L}(x). \end{aligned} \qquad (13)$$

In one dimension, coarsening is due to the unstable character of the periodic stationary configurations, *i.e.* to the existence of negative eigenvalues in the energy spectrum [22]. Because of the periodic character of the operator $D_x\hat{H}$, eigenvalues are grouped into bands.

Our evolution equation for $m(x,t)$ is $\partial_t m = D_x j$ where the current j (see Eq. (5)) can be derived from a pseudo free energy $\mathcal{F}$:

$$j = -\frac{\delta\mathcal{F}}{\delta m} \qquad \mathcal{F} = \int {\rm d}x \left[\tfrac{1}{2}(\partial_x m)^2 - V_{\rm ES}(m)\right]. \qquad (14)$$

For model 0 the potential $-V_{\rm ES}(m)$ has the standard double well shape and $m(x,t)$ evolves accordingly to the Cahn-Hilliard equation; in the presence of conserved noise we obtain the so-called model B of dynamics [23]. If D_x is replaced by the identity operator, the order parameter is no longer conserved and its evolution equation is $\partial_t m = j$, which is equivalent for model 0 to the time dependent Ginzburg Landau equation, or – in the presence of nonconserved noise – to model A of dynamics [23]. We use the notations $\tilde{\epsilon}, \tilde{\phi}$ for the spectrum of the operator $D_x\hat{H}$ and ϵ, ϕ for the Hamiltonian operator $\hat{H}$.

Let us start with few general statements on the lowest part of the spectrum. Translational invariance implies that $\epsilon = 0$ is always an eigenvalue of the operator $\hat{H}$ (and therefore $\tilde{\epsilon} = 0$ is an eigenvalue of $D_x\hat{H}$ as well) and it corresponds to the eigenfunction $\phi(x) = \tilde{\phi}(x) = m'_{\rm 2L}(x)$. To prove this let us use the definition of $m_{\rm 2L}(x)$ as a solution to the differential equation (7) and take the derivative:

$$m'''_{\rm 2L}(x) + j'_{\rm ES}(m_{\rm 2L})m'_{\rm 2L}(x) = 0 \ . \qquad (15)$$

Since $U_{\rm L}(x) = -j'_{\rm ES}(m_{\rm 2L}(x))$ we just have

$$-\partial_x^2(m'_{\rm 2L}(x)) + U_{\rm L}(x)(m'_{\rm 2L}(x)) \equiv \hat{H}m'_{\rm 2L}(x) = 0 \ . \qquad (16)$$

Therefore the operators $\hat{H}$ and $D_x\hat{H}$ have a zero energy eigenvalue and the corresponding eigenfunction $m'_{\rm 2L}(x)$ has period $\lambda = 2L$ (*i.e.* it corresponds to the wavevector $q = \pi/L$ in the Bloch representation).

We can now recognize the importance of the limit $m_\infty(x)$. If $m_\infty(x)$ exists, for $L \to \infty$ the periodic potential $U_{\rm L}(x)$ becomes a single well potential $U_\infty(x)$. In this limit $m_{\rm 2L}(x)$ is a monotonic function $m_+(x)$ (the kink solution, for model 0). Therefore $\tilde{\phi}_1(x) = \phi_1(x) \equiv m'_+(x)$ has no node and it represents the ground state for the single well problem. For finite L we have a periodic potential and the energy level $\epsilon_1 = \tilde{\epsilon}_1 = 0$ gives rise to the lowest band of the spectrum. The ground state $\epsilon_{\rm GS}(L)$ of the operator $\hat{H}$ corresponds to $q = 0$ and must therefore have a negative energy, implying that $\hat{H}$ has negative eigenvalues. The relation $\tilde{\epsilon}_{\rm GS} = \tilde{\epsilon}(q = 0)$ is no longer valid for the conserved model, but Langer [20] has shown that negative eigenvalues ϵ of $\hat{H}$ may be put in correspondence to negative eigenvalues $\tilde{\epsilon}$ of $D_x\hat{H}$ (see Sect. 4.1).

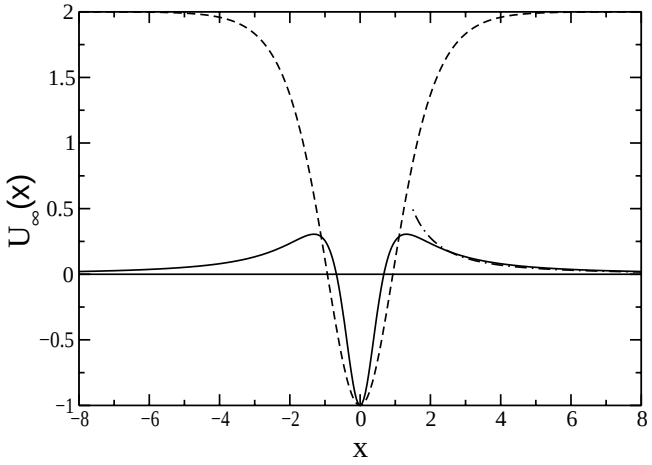

Fig. 2. The single well potential $U_\infty(x)$ for model 0 (dashed line) and for model $\alpha = 3$ (full line). At large x the former approaches 2, while the latter vanishes as $U_\infty(x) = a/x^2$, with $a = 10/9$ (dashed-dotted line, see formula (25)).

Since an unstable mode increases exponentially with the factor $\exp(|\epsilon|t)$, the knowledge of the L dependence of the ground state energy allows to find the deterministic coarsening law $L(t)$ *via* the relations $|\epsilon_{\rm GS}(L)| \sim 1/t$ (nonconserved model) and $|\tilde{\epsilon}_{\rm GS}(L)| \sim 1/t$ (conserved model).

4 Deterministic coarsening

In Figure 2 we plot the single well potentials $U_\infty(x)$ for model 0 (dashed line) and for model $\alpha = 3$ (full line), the latter being representative of all the class of α-models. Since, as already been explained, $\epsilon_1 = 0$ is the ground state energy for the single well, completely different behaviors are expected in the two cases.

For model 0 (see Sect. 4.1), $U_\infty(x)$ approaches 2 at large x: therefore the wavefunction $\phi_1(x)$ decays exponentially at large distances and energy shifts due to the tunneling between wells at finite distance L are expected to be exponentially small. This property is the counterpart of the exponentially vanishing interaction between kinks, discussed in Section 3.1.

For α-models (see Sect. 4.2), $U_\infty(|x| = \infty) = 0 = \epsilon_1$ and the considerations developed for model 0 do not apply.

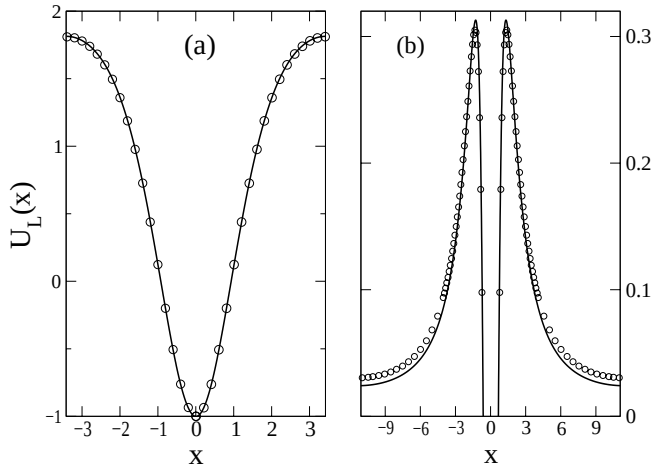

Fig. 3. The true periodic potential $U_{\rm L}(x)$ (empty circles) is compared with the potential $U^*_{\rm L}(x)$ (full line), obtained as a superposition of the single well potentials $U_\infty(x-nL)$ (see Eq. (18)). We make this comparison for model 0 (a), where $L \simeq 6.8$, and for model α =3 (b), where $L \simeq 22.8$. In both cases we display one period only. $U_{\rm L}(x)$ is obtained numerically and $U^*_{\rm L}(x)$ is obtained analytically. The superposition principle works well in (a) even for small L, while the exact potential for model 3 (see b) is *not* reproduced by the sum of single well potentials. In order to make more evident the difference between the two potentials, in (b) we focus the plot on the region of positive $U_{\rm L}(x)$. We remind that $U_{\rm L}(0) = -1$ for any α.

4.1 Model 0

For model 0 the kink-solution is $m_\infty(x) = \tanh(x/\sqrt{2})$, the single well potential is (see the dashed line in Fig. 2)

$$U_\infty(x) = -1 + 3m^2_\infty(x) = -1 + 3\tanh^2(x/\sqrt{2}) \qquad (17)$$

and the corresponding ground state wavefunction is $\phi_1(x) = m'_\infty(x) = \frac{1}{\sqrt{2}}\sec^2(\frac{x}{\sqrt{2}})$.

For finite L, $U_{\rm L}(x)$ is a collection of wells centred at points $x = 0, \pm L, \pm 2L, \ldots$. It is interesting to compare $U_{\rm L}(x)$ with the periodic potential $U^*_{\rm L}(x)$ obtained as a superposition of the single well potentials $U_\infty(x-nL)$:

$$U^*_{\rm L}(x) = U_\infty(x) + \sum_{n\neq 0}\left[U_\infty(x-nL) - U_\infty(\infty)\right]. \qquad (18)$$

For model 0, $U_\infty(\infty) = 2$ and the summation can indeed be limited to the two terms $n = \pm 1$ because the quantity in square brackets is exponentially small. In Figure 3a we show that $U^*_{\rm L}(x)$ (full line) is an excellent approximation of $U_{\rm L}(x)$ (circles).

Langer performed a tight-binding-approximation to determine the lowest band of the energy spectrum arising from the ground state $\epsilon_1 = 0$ of the single well. The result [20] is

$$\epsilon(q) \simeq -(1+\cos qL)\exp(-2L)\ , \qquad (19)$$

confirming that $\epsilon(q = \pi/L) = 0$, $\epsilon_{\rm GS} = \epsilon(q = 0)$ and that $\epsilon_{\rm GS}$ decays exponentially with the distance L between wells. The relation $|\epsilon_{\rm GS}| \sim 1/t$ [24] implies that coarsening is logarithmically slow: $L(t) \sim \ln t$. This result is valid for the *conserved* model as well. Langer proved it by means of the variational condition [20]:

$$\tilde{\epsilon}_{\rm GS} \leq \frac{\epsilon_{\rm GS}}{(\bar{\phi}_1, \phi_1)} \qquad (20)$$

where

$$(\bar{\phi}_1, \phi_1) = \int {\rm d}x \bar{\phi}^*_1(x)\phi_1(x) \qquad (21)$$

is the scalar product between the ground state function $\phi_1(x)$ of the Hamiltonian operator and $\bar{\phi}_1$ is defined by the relation $D_x\bar{\phi}_1 = \phi_1$.

Because of the conservation law, the lowest energy band for the operator $D_x\hat{H}$ reads [20]:

$$\epsilon(q) \simeq -\sin^2 qL \times \frac{\exp(-2L)}{L}\ . \qquad (22)$$

The factor L in the denominator is irrelevant and the coarsening law $L(t) \sim \ln t$ is still valid. Equation (22) also confirms that $\tilde{\epsilon}(q = \pi/L) = 0$ and that $\tilde{\epsilon}(q = 0)$ is no more the ground state.

4.2 α-models

The solution of model 0 by Langer is of great interest because it gives approximate expressions for the lowest energy band, both for the nonconserved (19) and conserved (22) models. The basis of his treatment is the tight-binding-approximation: $\Delta U(x) \equiv U^*_{\rm L}(x) - U_\infty(x)$ is taken as a small perturbation of $U_\infty(x)$.

In the case of α-models, a simpler strategy can be followed [12] by replacing the periodic potential $U_{\rm L}(x)$ with a double well $U_2(x)$, obtained by joining rather than superposing $U_\infty(x)$ and $U_\infty(x-L)$ [25]. Using this approximation, our analytical results for the coarsening exponent $n(\alpha)$ agree well with the estimate obtained from numerical integration of the growth equations [12] (see the results for the conserved model reported in Fig. 9). In the following we report the general lines of this theoretical approach, and we add a direct numerical confirmation (see Fig. 4).

The single well potential $U_\infty(x)$ for the α-models (see Fig. 2) decays to zero at large x from positive values. From the relation $U_\infty(x) = -j'_{\rm ES}(m_\infty(x))$ it is simple to derive that for $m \gg 1$:

$$U_\infty(x) \sim \frac{(2\alpha-1)}{m^{2\alpha}_\infty(x)}\ . \qquad (23)$$

The integration of Newton's equation (7) for zero energy gives the asymptotic result ($x \gg 1$):

$$m^\alpha_\infty(x) \sim \tfrac{\alpha}{\sqrt{\alpha-1}}x, \qquad (24)$$

which implies

$$U_\infty(x) \sim \frac{(2\alpha-1)(\alpha-1)}{\alpha^2}\frac{1}{x^2} \equiv \frac{a}{x^2}\ . \qquad (25)$$

Table 1. The deterministic coarsening exponent n, for the nonconserved ($D_x \equiv 1$) and the conserved ($D_x \equiv -\partial_x^2$) models. For $\alpha = 2$ there are logarithmic corrections (see [12]).

	$1 < \alpha < 2$	$\alpha > 2$
nonconserved	$\frac{1}{2}$	$\frac{\alpha}{3\alpha-2}$
conserved	$\frac{1}{4}$	$\frac{\alpha}{5\alpha-2}$

Thus the single well potential decays as the inverse of a square law *whatever* the value α, but with a prefactor a that increases between $a = 0$ for $\alpha = 1$ and $a = 2$, for $\alpha = \infty$. For $\alpha = 3$, $a = \frac{10}{9}$ and the corresponding function $\frac{a}{x^2}$ is reported in Figure 2 as the dashed-dotted line, showing the comparison between the asymptotic expansion (25) and the exact expression [26].

The solution $\phi_1(x)$ of the Schrödinger equation for the single well (let us remind that the ground state has zero energy) therefore decays at large x as a power law [12]: $\phi_1(x) \sim |x|^{-\beta}$, with $\beta = (1 - \alpha^{-1})$. So, the ground state wavefunction is a bound state for $\beta > \frac{1}{2}$ *i.e.* $\alpha > 2$ only.

In reference [12] we used the Landau and Lifshitz approach [27] for the double-well problem and we extended it to take into account the possibility that the ground state wavefunction for the single well is not a bound state. This happens for $1 < \alpha \leq 2$. The main point is that even if $\phi_1(x)$ is not a bound state, the ground state $\phi_2(x)$ of the double well *is* bound, because its energy ϵ_2 is now strictly negative and so lower than the asymptotic value $U_2(\infty) = 0$.

Following the above approach we found [12] that

$$|\epsilon_{\rm GS}(L)| \simeq L^{-\gamma} \qquad \gamma = \begin{cases} 2 & \alpha < 2 \\ (3 - \frac{2}{\alpha}) & \alpha > 2 \end{cases} . \qquad (26)$$

Once γ is known, the coarsening exponent n is just given by $n = 1/\gamma$. In Table 1 we summarize the results found in reference [12] for the nonconserved and conserved models. For $\alpha = 2$ there are logarithmic corrections: $L \sim (t/\ln t)^n$.

The reason why it has not been possible to treat the periodic potential $U_{\rm L}(x)$ in a more rigorous way is given in Figure 3b, where it is clearly shown that the superposition principle does *not* work for α-models: accordingly, the potential $U_{\rm L}(x)$ can not be approximated as the sum of single-well potentials. Therefore, the application of the tight-binding-approximation is not straightforward because we do not know the explicit expression of the perturbation $\Delta U(x) \equiv U_{\rm L}(x) - U_\infty(x)$. The disagreement between $U_{\rm L}(x)$ and $U_{\rm L}^*(x)$ might appear at first sight to be unimportant, but if we neglect their difference we obtain wrong results (as we have verified).

However, it is possible to check *in a direct way* the accuracy of our theory: we solve numerically the quantum mechanical problem to determine the ground state energy $\epsilon_{\rm GS}(L)$ of the full periodic potential $U_{\rm L}(x)$ (see Fig. 4 and footnote [28]). The numerical results for the exponent γ agree fairly well, at large L, with the theoretical predictions $\gamma(3) = 2.33$ and $\gamma(10) = 2.8$. This confirms that our theoretical approach to calculate $\epsilon_{\rm GS}(L)$ is indeed correct.

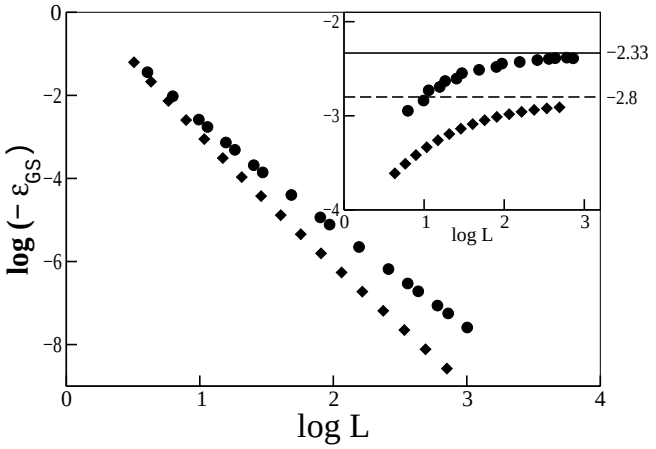

Fig. 4. Nonconserved models: on a log-log scale (main) we report the absolute value of the ground state energy $\epsilon_{\rm GS}(L)$ for the periodic potential $U_{\rm L}(x)$. Circles refer to model 3 and diamonds to model 10. In the inset we report the local derivatives $d[\log(-\epsilon_{\rm GS})]/d[\log(L)]$ and the asymptotic values of γ that are calculated analytically (see Eq. (26)).

4.3 Numerical analysis

Let us now discuss our numerical results for the deterministic α-models. We have numerically integrated the equation of motion (4) with $\eta = 0$, starting from an initial profile $z(x, 0) = r_x$, where r_x is a random variable with a flat distribution in the interval $[-0.1, 0.1]$.

Typically, we have followed the dynamical evolution for a total time $t_{\rm MAX} \sim 400,000 - 1,600,000$, for a chain length $L_c = 1024$, with a spatial resolution $\delta x = 0.25$ and an integration time step $\tau = 0.05$. A few tests have also been performed with a smaller time step $\tau = 0.025$ and with longer chains ($L_c = 2048 - 4096$), obtaining consistent results. The adopted integration scheme is a time-splitting pseudo-spectral code: more details are reported in Appendix A.1.

At the top of Figure 5 we display a portion of the surface profile $z(x)$ for the model $\alpha = 3$. It appears to be made up of regions of constant slope separated by domain walls. However, the slope profile $m(x)$ reported in the centre of Figure 5 does not corroborate this picture: no region of constant slope is clearly visible and the maxima or minima have appreciably different values. The same remark is applicable at later times. On the bottom of Figure 5 we also display the potential $U(x) = -j'_{\rm ES}(m(x))$ that enters into the analytical solution of the problem (see the previous section). It is therefore reassuring that $U(x)$ looks indeed as a regular sequence of the single well potentials depicted in Figure 2 as a full line, because it confirms that the surface profile keeps close to a stationary configuration.

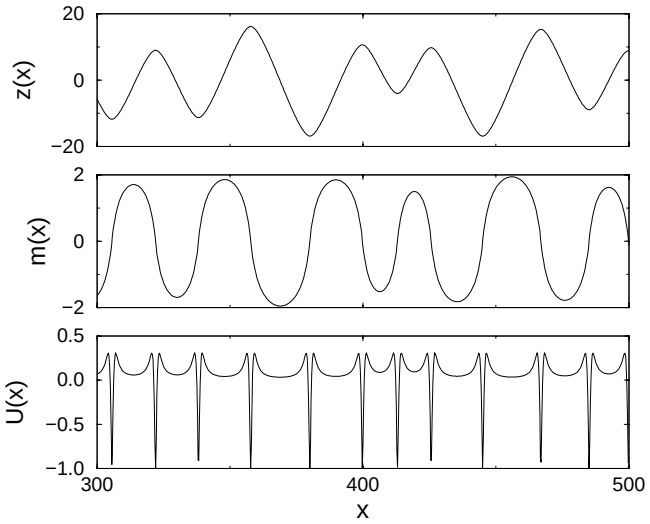

Fig. 5. Model $\alpha = 3$, late stages of coarsening. Top: the surface profile $z(x)$ as obtained *via* numerical integration. Centre: the slope profile $m(x) = z'(x)$. Bottom: the potential $U(x) = -j'_{\rm ES}(m)$. We display only a piece of the total spatial domain.

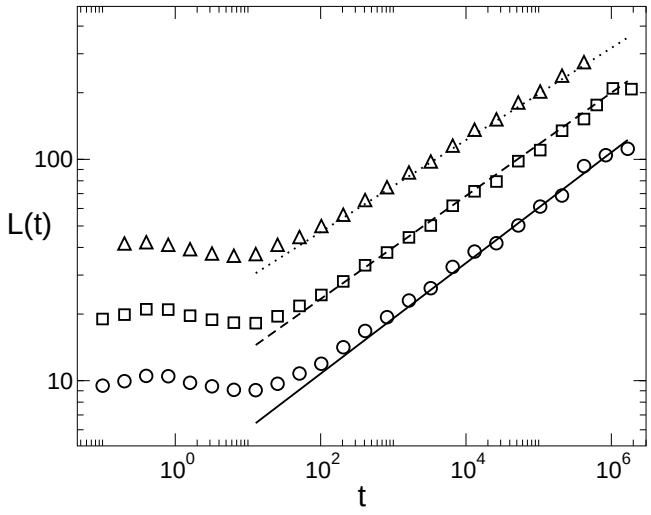

Fig. 6. Deterministic coarsening: L *vs.* t in log-log scale for $\alpha = 1.5$ ($\circ$), $\alpha = 3$ ($\square$) and $\alpha = 10$ ($\triangle$). For presentation purpose the data for $\alpha = 3$ and 10 are shifted by a constant. The lines indicate the best fit to the data for $t > 10,000$ and the slopes are equal to 0.250 (—), 0.233 (- - -) and 0.208 ($\cdots$), in agreement with the theoretical prediction (see Tab. 1).

The next step is to evaluate the characteristic length $L(t)$, corresponding to the average distance between wells. We define the wavevector $p_c(t)$ *via* the relation:

$$p_c(t) = \frac{\sum'_p pS(p,t)}{\sum'_p S(p,t)}, \tag{27}$$

where $S(p,t) = |\tilde{z}(p,t)|^2$ is the power spectrum associated with the field z at time t ($\tilde{z}$ being its spatial Fourier transform) and the sum is restricted to the wavevectors p for which $S(p) \geq \delta \times S_{\rm M}$, $S_{\rm M}$ being the maximum value of the spectrum and δ some threshold (typical values are $\delta \sim 0.1 - 0.2$). The characteristic length is then evaluated as $L(t) = 2\pi/p_c(t)$ and the coarsening exponent $n(\alpha)$ has been obtained by considering the scaling behavior of $L(t) \sim t^n$ in a time interval $10,000 < t < 400,000 - 1,600,000$.

As an independent check we have also determined L from the normalized spatial correlation function of the surface profile

$$C(r,t) = \frac{\langle z(x+r,t)z(x,t)\rangle - \langle z(x,t)\rangle^2}{\langle z(x,t)^2\rangle - \langle z(x,t)\rangle^2}, \tag{28}$$

where the spatial average $\langle\cdot\rangle$ is performed along the chain. Defining L by the relation

$$C(L,t) = C(0,t)/2 \tag{29}$$

our results are in agreement with the previous ones obtained from the power spectrum in all the considered cases.

The numerically estimated length $L(t)$ is reported in Figure 6 for $\alpha = 1.5, 3, 10$. The coarsening exponents are $n(1.5) = 0.250 \pm 0.003$, $n(3) = 0.233 \pm 0.005$ and $n(10) = 0.208 \pm 0.002$. These results are consistent with the theoretical estimates for $n(\alpha)$, as summarized in Figure 9. Their critical discussion is deferred to the final section.

5 Coarsening with conservative noise

The stochastic equation (4) has been integrated up to a time $t_{\rm MAX} \sim 800,000$ with $L_c = 1024$. The results for $L(t)$ and $C(r,t)$ have been obtained by averaging over N_c different initial conditions with different noise realizations (typically $N_c = 10$). The integration scheme employed in the noisy case is different from the one adopted for the deterministic case and it is described in detail in Appendix A.2. We have used a noise strength corresponding to a value of $\tilde{F}_0$ (see Eq. (6)) equal to 0.05. This is a physically reasonable value because for large ES barriers [5], $\tilde{F}_0 \approx \frac{a}{\ell_{\rm D}}$ and $\ell_{\rm D}$ is typically of the order of a few dozens of lattice constants.

For the noisy case we have defined L only in term of the average correlation function $\overline{C(r,t)}$, where the bar means that the average is now performed at each time not only along the chain (see definition (28)) but also over different noise realizations. A sufficiently good scaling is obtained in the time interval $40,000 < t < 800,000$ for all the considered values of α ($= 1, 2, 10$).

As a benchmark to verify the validity both of our integration scheme and of our procedure to estimate $n(\alpha)$, we have analyzed model 0. In this case the coarsening exponent is known [19,20] to be $n = 1/3$. A good agreement between our numerical data and the theoretical prediction is found for $t > 40,000$, as shown in Figure 7.

For the two values of α, $\alpha = 1$ and $\alpha = 10$, we find $n = 1/4$. We conclude that, in the presence of shot noise,

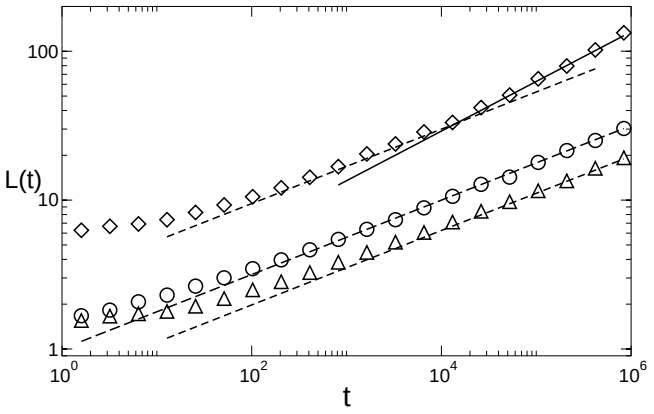

Fig. 7. Coarsening in the presence of shot noise: L *vs.* t in log-log scale for model 0 ($\Diamond$) and for $\alpha = 1$ ($\triangle$) and $\alpha = 10$ ($\circ$). Dashed lines have slope 1/4 and full line has slope 1/3.

the coarsening exponent is independent of α and equal to 1/4. Figure 7 also suggests the possible existence for model 0 of an intermediate regime (with $L \sim 5 - 20$) where an effective exponent $n = \frac{1}{4}$ is found.

6 Effects of a symmetry breaking term

In reference [17] one of us studied the effect of symmetry breaking on model 0. Since in that model the slope keeps finite with a maximal value equal to one, the detailed expression of the function $A(m^2)$ ($j_{\rm SB} = \partial_x A$) is not relevant. The simplest form, was therefore chosen the one valid at small slopes: $A(m^2) = \lambda^* m^2$.

On the contrary, for α-models the slope can diverge so that the exact expression of $j_{\rm SB}$ should be used [14]:

$$j_{\rm SB} = -\lambda^* \partial_x \left(\frac{1}{1+m^2} \right) \cdot \tag{30}$$

We limited ourselves to the physically relevant case $\alpha = 1$. We have therefore integrated the following differential equation:

$$\partial_t z = -\partial_x \left[\partial_x^2 m + \frac{m}{1+m^2} - \lambda^* \partial_x \left(\frac{1}{1+m^2} \right) \right] + \eta \tag{31}$$

for values of λ^* varying between 0.1 and 1.

Our results (see Fig. 8) suggest that $j_{\rm SB}$ is *irrelevant* for the coarsening law, both for $\eta \equiv 0$ (deterministic case) and for $\eta \neq 0$ (noisy case).

7 Discussion and conclusions

In Figure 9 we have summarized our numerical and theoretical results for the coarsening exponent n ($L \sim t^n$). In the absence of noise, our theory (full line) predicts that $n = \frac{1}{4}$ for $1 < \alpha \leq 2$ and for larger values of α it decreases down to $\frac{1}{5}$ ($n = 1/(5 - \frac{2}{\alpha})$). Numerical results (full circles) agree well with the full fine.

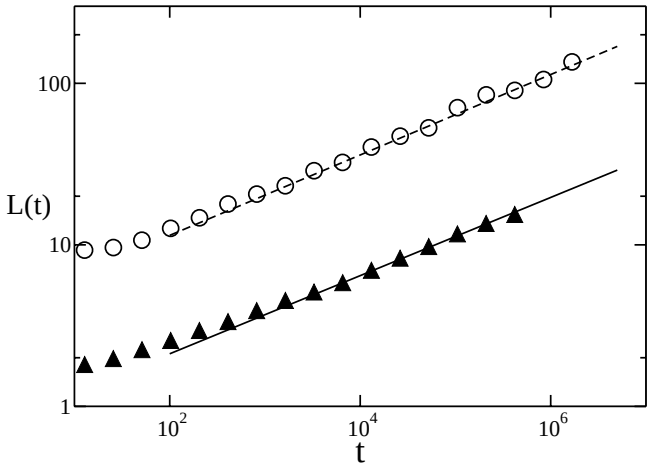

Fig. 8. Coarsening for the asymmetric model (Eq. (31) with $\lambda^* = 1$), in the absence (empty circles) and in the presence (full triangles) of shot noise. Fits have been made for $t > 10^4$ and give $n = 0.25$ without noise (dashed line) and $n = 0.24$ with noise (full line). Circles have been shifted by a constant.

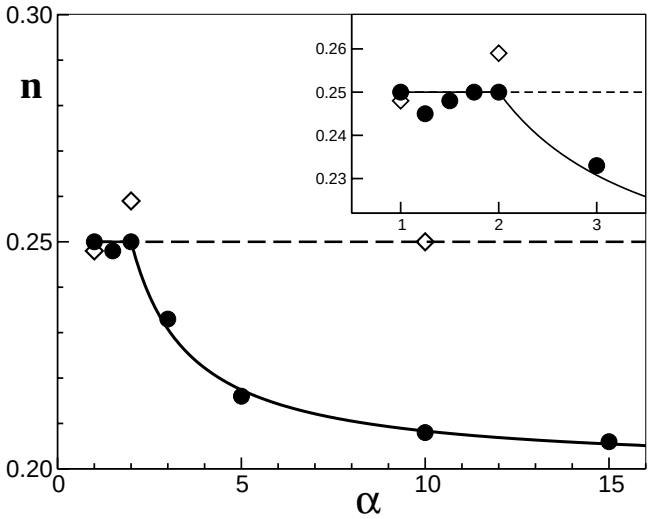

Fig. 9. The coarsening exponent n as a function of α, for the deterministic models (full circles) and for the stochastic models (open diamonds). In the inset we enlarge the region of small α. Full line is the theoretical result in the absence of noise (Tab. 1) and the dashed line is our ansatz $n = 1/4$ for the noisy case.

We are aware of only one analytical paper treating our class of models (Ref. [29]). The author uses scaling arguments to conclude that, *in the absence* of noise, $n = 1/4$ irrespectively of α and for any dimension d of the substrate. In the following we give a drastically simplified version of the scaling arguments. If Z, L and $M = Z/L$ are respectively the typical height, width and slope of mounds at time t, the evolution equation for $z(x,t)$ implies $Z/t \sim j/L$. The current j is made up of the Mullins term, of order M/L^2 plus the ES current, whose asymptotic expression for large slope is $1/M^{2\alpha-1}$. They vanish in the limit $t \to \infty$ and must be of the same order in $\frac{1}{t}$, which entails the relation $M^\alpha \sim L$. If their sum j is supposed to be of

the same order as well, the relation $Z/t \sim M/L^3$ implies $L(t) \sim t^{1/4}$, *i.e.* $n = 1/4$ for any α.

One main drawback of the scaling argument is that the two terms appearing in j are of the same order but their sum is smaller (*i.e.* of higher order in $\frac{1}{t}$) because of a compensation effect. This is a necessary condition for the stationary configurations to play a role in the coarsening process.

In order to have a direct numerical check of our statement, we have evaluated the quantities $\langle|\partial_x j_{\rm M}|\rangle$, $\langle|\partial_x j_{\rm ES}|\rangle$ and $\langle|\partial_x(j_{\rm M} + j_{\rm ES})|\rangle$, as a function of time, where $\langle\cdots\rangle$ means, as before, the spatial average. For all the considered values of α ($\alpha = 1, 3, 10$), the result is the same: the ratio $\langle|\partial_x j_{\rm M}|\rangle/\langle|\partial_x j_{\rm ES}|\rangle$ is equal to one, up to higher order terms, and $\langle|\partial_x(j_{\rm M} + j_{\rm ES})|\rangle/\langle|\partial_x j_{\rm M}|\rangle$ vanishes.

Our numerical results tell even more than that: in fact scaling arguments would suggest that n is strictly smaller than $\frac{1}{4}$ if j is smaller than $j_{\rm M}$ and $j_{\rm ES}$, but for $\alpha \leq 2$ we do find $n = \frac{1}{4}$ even if $|j|/|j_{\rm M}| \simeq |j|/|j_{\rm ES}| \to 0$.

Model $\alpha = 1$ had been previously studied numerically at short times also in reference [30] and authors found a value $n \approx 0.22$, independent of the noise strength.

Let us now discuss the results in the presence of noise. Figure 9 presents with diamonds the numerical results for the stochastic integration of equation (4). Our data refer to $\alpha = 1, 2, 10$ and provide reasonably convincing evidence that in the presence of noise the coarsening exponent remains constant, $n = \frac{1}{4}$ (dashed line). The somewhat larger value for $\alpha = 2$ may be due to unknown logarithmic corrections.

Authors in references [31,32] use qualitative arguments to describe coarsening assisted by noise: they use a 'single mound' model and find the coarsening time by requiring that shot noise induces a height fluctuation of the same order of the mound height. In one dimension they find $n = 1/(3+\frac{2}{\alpha})$, where α is defined phenomenologically through the asymptotic relation $M \sim L^{1/\alpha}$ between the typical (or the maximal) slope M and the width L of mounds.

Their prediction for $n(\infty)$ seems to agree with the result $n = \frac{1}{3}$ for model 0. This is reasonable because in that model the slope is constant and therefore it can effectively be equivalent to the model $\alpha = \infty$. Actually, if we take the limit $\alpha = \infty$ in equation (5), it is straightforward to conclude that the current $j_{\rm ES}$ vanishes and we obtain the linear equation:

$$\partial_t z(x,t) = -\partial_x^4 z(x,t) + \eta(x,t). \tag{32}$$

The basic question is whether our class of α-models tends – in some sense – to equation (32) with increasing α. In the absence of noise, the answer is surely negative: indeed, equation (32) does not admit stationary periodic solutions that, as discussed above, are crucial for deterministic coarsening.

On the other hand, if noise is present ($\eta \neq 0$), equation (32) describes a process of kinetic roughening: the growing surface is characterized by a correlation length $\tilde{\xi}(t) \sim t^{1/\tilde{z}}$, where $\tilde{z}$ is the dynamical critical exponent. In $d = 1$ it is well known [4] that for the quartic linear equation (32), $\tilde{z} = 4$. It is reasonable to assume that the stochastic α-model does converge to equation (32) for $\alpha \to \infty$ and –in the same limit– $n(\alpha) \to \frac{1}{\tilde{z}} = \frac{1}{4}$.

The meaning of a constant value $n = \frac{1}{4}$ for any α is simple: in the presence of noise the detailed form of the current $j_{\rm ES}$ is irrelevant provided that the slope m diverges.

We can now summarize our main results. Without noise, $n = \frac{1}{4}$ for $\alpha \leq 2$ and $n = 1/(5 - \frac{2}{\alpha})$ for $\alpha > 2$. This result has been obtained analytically and it has been confirmed by extensive numerical calculations. It can not be deduced by simple scaling arguments. In the presence of noise our numerical data for $\alpha = 1, 2, 10$ suggest that $n = \frac{1}{4}$ irrespectively of α. This assume agrees with the well known result $\tilde{\xi}(t) \sim t^{1/4}$, valid for the linear model $\alpha = \infty$. So, steepening of mounds makes coarsening faster without noise and slower with noise.

We believe that the surface profile can not be described as a sequence of mounds with a spatially constant slope M that increases in time (see Fig. 5, centre). This wrong assumption may be the reason why qualitative arguments to determine n do fail.

We have also considered the possible effect of a symmetry breaking term $j_{\rm SB}$ in the current: it is irrelevant for model 1, as already proved for model 0 [17].

We conclude the paper by mentioning a different model, whose coarsening properties bear some similarities with our α-models. It has been studied by Bray and Rutenberg [33] and it includes in the addition of a long-range attraction between kinks to model 0. If such an interaction decays as a power law of the distance ($1/L^s$, with $s > 1$) the deterministic coarsening exponent is found to be $n = 1/(1 + s)$. In the presence of conservative noise, this appears to be relevant for $s > 2$ and in that case $n = \frac{1}{3}$. Some analogies therefore exist with our class of α-models, because in both cases the coarsening exponent is a continuously varying function of a parameter (α or s), noise may be relevant ($\alpha, s > 2$) or not ($1 < \alpha, s \leq 2$), and –finally– the stochastic coarsening exponent is constant if noise is relevant.

We warmly thank C. Castellano for a detailed and critical reading of the manuscript. We also acknowledge useful discussions with A. Crisanti and D. Mukamel. The authors would like to thank S. Lepri and M. Moraldi for their revision of the manuscript.

Appendix A: Integration algorithms

Let us rewrite in an explicit way the evolution equation (4) for the field $z(x,t)$:

$$\partial_t z(x,t) = -\partial_x^4 z - \partial_x \left[\frac{\partial_x z}{(1 + (\partial_x z)^2)^\alpha}\right] + \eta(x,t), \tag{A.1}$$

where $\eta(x,t)$ indicates additive δ-correlated spatio-temporal Gaussian noise, *i.e.*

$$\langle\eta(x,t)\rangle = 0 \tag{A.2}$$

$$\langle\eta(x,t)\eta(0,0)\rangle = \tilde{F}_0\delta(x)\delta(t). \tag{A.3}$$

A.1 Deterministic equation

Let us first neglect the noise term: in order to perform the numerical integration of (A.1) we consider a discrete spatial grid of resolution δx and a discrete time evolution with time step τ. The discretized field is written as $z(i,n)$, where the integer indices i and n are the spatial and temporal discrete variables, respectively. Periodic boundary conditions have been considered for the field: $z(i,n) = z(i+I,n)$, where I is the number of sites of the grid ($L_c = I\delta x$). The algorithm adopted to integrate (A.1) is a time-splitting pseudo-spectral code [34]. In particular, by following [35] equation (A.1) has been rewritten as

$$\partial_t z(x,t) = (\mathcal{L}+\mathcal{N})z(x,t) \tag{A.4}$$

where $\mathcal{L}$ and $\mathcal{N}$ are two operators defined in the following way: $\mathcal{L}z = -\partial_x^4 z$ and $\mathcal{N}z = -\partial_x\left[\frac{\partial_x z}{(1+(\partial_x z)^2)^\alpha}\right]$. As usual for time splitting algorithms, the linear evolution, ruled by the operator $\mathcal{L}$, is treated independently from the nonlinear one (associated to the operator $\mathcal{N}$). A complete evolution over an integration time step τ therefore corresponds to the two successive integration steps:

$$z^*(x,t+\tau) = \exp[\mathcal{L}\tau]z(x,t) \tag{A.5}$$

and

$$z(x,t+\tau) = \exp[\mathcal{N}\tau]z^*(x,t+\tau) \tag{A.6}$$

where $z^*(x,t)$ is a dummy field.

Let us initially consider the linear part,

$$\partial_t z(x,t) = \mathcal{L}z(x,t)\ . \tag{A.7}$$

Equation (A.7) can be easily solved in Fourier space and the equation of motion for the spatial Fourier transform of the field $\tilde{z}(p,t)$ is

$$\partial_t \tilde{z}(p,t) = -p^4\tilde{z}. \tag{A.8}$$

The time evolution for $\tilde{z}$ is simply given by

$$\tilde{z}^*(p,t+\tau) = \exp[-p^4\tau]\tilde{z}(p,t). \tag{A.9}$$

Therefore, in order to integrate equation (A.7), the field should be Fourier transformed in space ($\mathcal{F}$), then multiplied by the propagator reported in equation (A.9) and the outcome of such an operation should be finally inverse-Fourier transformed ($\mathcal{F}^{-1}$):

$$z^*(x,t+\tau) = \mathcal{F}^{-1}\exp[-p^4\tau]\mathcal{F}z(x,t)\,. \tag{A.10}$$

The integration of the nonlinear part has been performed by employing a second-order Adam-Basforth scheme

$$z(x,t+\tau) = z^*(x,t+\tau) + \frac{\tau}{2}\left[3\,G(z(x,t)) - G(z(x,t-\tau))\right], \tag{A.11}$$

where $G(z(x,t)) = \left\{-\partial_x\left[\frac{\partial_x z}{(1+(\partial_x z)^2)^\alpha}\right]\right\}$. In order to obtain better precision, the spatial derivatives appearing in $G(z(x,t))$ have been evaluated in Fourier space.

A.2 Stochastic equation

Let us now consider the noisy problem: in this case the algorithm outlined here above does not guarantee sufficient precision. Therefore, we have developed a more accurate integration scheme [36] that consists, as a first step, of rewriting the equation of motion (A.1) in the Fourier space

$$\partial_t\tilde{z}(p,t) = -p^4\tilde{z}(p,t) + G_p(z,t) + \tilde{\eta}(p,t), \tag{A.12}$$

where $G_p(z,t)$ and $\tilde{\eta}(p,t)$ are the Fourier transforms of the nonlinear part and of the noise term appearing in equation (A.1). The amplitudes $\tilde{\eta}(p,t)$ of the noise components in the Fourier space are still Gaussian δ-correlated stochastic variables with zero average and with a variance $\mathcal{V}_p = \mathcal{F}_0/I$ independent of p (white noise). The formal exact solution of (A.12) is

$$\tilde{z}(p,t+\tau) = \mathrm{e}^{-p^4\tau}\left[\tilde{z}(p,t) + \int_t^{t+\tau}\mathrm{d}t'\,\mathrm{e}^{p^4(t'-t)}(G_p(z,t') + \tilde{\eta}(p,t'))\right]. \tag{A.13}$$

The problem now is to evaluate the two terms appearing in the integral. The first term has been evaluated adopting a second order Adam-Bashfort scheme, *i.e.*

$$\int_t^{t+\tau}\mathrm{d}t'\,\mathrm{e}^{p^4(t'-t)}G_p(z,t') = \frac{\tau}{2}\left[3G_p(z,t) - \mathrm{e}^{-p^4\tau}G_p(z,t-\tau)\right] + \mathcal{O}(\tau^3)\,. \tag{A.14}$$

The treatment of the second term is more delicate, since it is a stochastic integral: we have chosen to evaluate it according to Ito's prescription [37]:

$$\int_t^{t+\tau}\mathrm{d}t'\,\mathrm{e}^{p^4(t'-t)}\tilde{\eta}(p,t') = [W_p(t+\tau) - W_p(t)] = \Delta W_p(t). \tag{A.15}$$

Here $W_p(t)$ and $\Delta W_p(t)$ represent two Wiener processes: in particular we have $\langle\Delta W_p\rangle = 0$ and $\langle(\Delta W_p)^2\rangle = \tau\mathcal{V}_p$. The complete solution of (A.12) can be written as

$$\tilde{z}(p,t+\tau) = \mathrm{e}^{-p^4\tau}\tilde{z}(p,t) + \frac{3\tau}{2}\mathrm{e}^{-p^4\tau}G_p(z,t) - \frac{\tau}{2}\mathrm{e}^{-2p^4\tau}G_p(z,t-\tau) + \mathrm{e}^{-p^4\tau}\Delta W_p(t). \tag{A.16}$$

In order to obtain the solution real space it is sufficient to inverse-Fourier transform $\tilde{z}(p,t+\tau)$.

Due to the spatial and temporal discreteness of the integration scheme, the spatio-temporal noise term $\eta(x,t)$ should be rewritten as γ_i^n, where γ is a random Gaussian variable of zero average and variance

$$\mathcal{V} = \frac{\tau\tilde{F}_0}{\delta x}, \tag{A.17}$$

with

$$\langle \gamma_i^n \gamma_0^0 \rangle = \mathcal{V} \delta_{i,0} \delta_{n,0}. \quad \text{(A.18)}$$

The spatio-temporal discrete Gaussian noise, with zero average and standard deviation $\sqrt{\frac{\tau \tilde{F}_0}{\delta x}}$ has been numerically generated by employing a Box-Muller algorithm [34].

References

1. A. Chame, S. Rousset, H.P. Bonzel, J. Villain, Bulg. Chem. Commun. **29**, 398 (1996/97) and references therein.
2. O. Pierre-Louis, C. Misbah, Y. Saito, J. Krug, P. Politi, Phys. Rev. Lett. **80**, 4221 (1998).
3. K. Kyuno, G. Ehrlich, Surf. Sci. **383**, L766 (1997) and references therein.
4. A. Pimpinelli, J. Villain, *Physics of crystal growth* (Cambridge, Cambridge University Press, 1998).
5. P. Politi, G. Grenet, A. Marty, A. Ponchet, J. Villain, Phys. Rep. **324**, 271 (2000).
6. M. Siegert, Physica A **239**, 420 (1997); M. Siegert, Phys. Rev. Lett. **81**, 5481 (1998); D. Moldovan, L. Golubovic, Phys. Rev. E **61**, 6190 (2000).
7. A.J. Bray, Adv. Phys. **43**, 357 (1994).
8. J. Krug, Adv. Phys. **46**, 139 (1997).
9. J. Villain, J. Phys. I France **1**, 19 (1991).
10. J.G. Amar, F. Family, Phys. Rev. Lett. **77**, 4584 (1996).
11. J.W. Evans, Phys. Rev. B **43**, 3897 (1991).
12. P. Politi, A. Torcini, J. Phys. A **33**, L77 (2000).
13. W.W. Mullins, J. Appl. Phys. **28**, 333 (1957).
14. P. Politi, J. Villain, Phys. Rev B **54**, 5114 (1996).
15. P. Politi, J. Villain, in *Surface Diffusion: atomistic and collective processes*, edited by M.C. Tringides (Plenum Press, New York, 1997) p. 177.
16. Z. Rácz, M. Siegert, D. Liu, M. Plischke, Phys. Rev. A **43**, 5275 (1991).
17. P. Politi, Phys. Rev. E **58**, 281 (1998).
18. A linear stability analysis of a 1d vicinal surface of constant slope m^* shows that step-flow is stable if $j'_{\rm ES}(m^*) < 0$.
19. K. Kawasaki, T. Ohta, Physica A **116**, 573 (1982); K. Kawasaki, T. Nagai, Physica A **121**, 175 (1983); T. Kawakatsu, T. Munakata, Prog. Theor. Phys. **74**, 11 (1985); T. Nagai, K. Kawasaki, Physica A **134**, 483 (1986).
20. J.S. Langer, Ann. Phys. **65**, 53 (1971).
21. S.J. Cornell, K. Kaski, R.B. Stinchcombe, Phys. Rev. B **44**, 12263 (1991).
22. Strictly speaking negative eigenvalues are a necessary but not a sufficient condition to ensure coarsening.
23. P.C. Hohenberg, B.I. Halperin, Rev. Mod. Phys. **49**, 435 (1977).
24. The exact relation, as derived by Langer [20] is $t^{-1} = \sum_q |\epsilon(q, L)|$ where the sum is restricted to the negative (and therefore unstable) modes. However, the L dependence of ϵ can be pulled out the summation and it is therefore sufficient to consider the ground state energy.
25. Joining means that $U_2(x) = U_\infty(x)$ for $x \leq \frac{L}{2}$ and $U_2(x) = U_\infty(x - L)$ for $x \geq \frac{L}{2}$. This kind of juxtaposition is used by Landau and Lifshitz [27] in their treatment of the double well problem and for model 0 it gives the correct results.
26. The Newton's equation for the model $\alpha = 3$ can be easily integrated if the particle has zero energy and therefore an explicit expression for $U_\infty(x)$ is available. We do not report it here, but we write explicitly the first correction to the leading order in the large x expansion: $U_\infty(x) \simeq \frac{10}{9x^2} + (\frac{16}{9})^{1/3} \frac{1}{x^{8/3}}$. At $x = 10$ the first correction is of order of one quarter of the leading term.
27. L.D. Landau, E.M. Lifshitz, *Quantum mechanics: non-relativistic theory* (Oxford, Pergamon Press, 1977), Section 50, Problem 3.
28. In order to find the ground state energy we have imposed periodic boundary conditions and searched for the zero node wavefunction. Precision real∗16 has been necessary in order to achieve a sufficient accuracy at large L.
29. L. Golubović, Phys. Rev. Lett. **78**, 90 (1997).
30. A.W. Hunt, C. Orme, D.R.M. Williams, B.G. Orr, L.M. Sander, Europhys. Lett. **27**, 611 (1994); L.M. Sander, private communication.
31. J. Krug, in *Nonequilibrium statistical mechanics in one dimension*, edited by V. Privman (Cambridge University Press, Cambridge, 1997), p. 305.
32. Lei-Han Tang, P. Šmilauer, D.D. Vvedensky, Eur. Phys. J. B **2**, 409 (1998).
33. A.J. Bray, A.D. Rutenberg, Phys. Rev. E **49**, R27 (1994); A.D. Rutenberg, A.J. Bray, Phys. Rev. E **50**, 1900 (1994). Different coarsening models in 1d are also studied in: S.N. Majumdar, D.A. Huse, Phys. Rev. E **52**, 270 (1995).
34. W.H. Press, *et al.*, *Numerical Recipes* (Cambridge University Press, Cambridge, 1992).
35. D. Goldman, L. Sirovich, Quart. Appl. Math. **53**, 315 (1995); A. Torcini, H. Frauenkron, P. Grassberger, Phys. Rev. E **55**, 5073 (1997); M. Nitti, A. Torcini, S. Ruffo, Int. J. Mod. Physics C **10**, 1039 (1999).
36. A. Crisanti, private communication
37. C.W. Gardiner, *Handbook of Stochastic Methods for Physics, Chemistry and the Natural Sciences* (Springer-Verlag, 1983, Berlin)